

# Advancement in Predictive Modeling of Mild Steel Corrosion in CO<sub>2</sub>- and H<sub>2</sub>S-Containing Environments

Yougui Zheng,\* Jing Ning,\* Bruce Brown,\* and Srdjan Nešić<sup>‡,\*</sup>

## ABSTRACT

Over the past decade, the knowledge related to predicting internal pipeline corrosion for sweet and particularly sour environments has dramatically improved. Advancement in understanding of the corrosion mechanisms related to H<sub>2</sub>S corrosion environments enabled the development of an integrated electrochemical model for CO<sub>2</sub>/H<sub>2</sub>S uniform corrosion, including the effect of H<sub>2</sub>S on the protective corrosion product formation on mild steel. The latest model of uniform CO<sub>2</sub>/H<sub>2</sub>S corrosion of carbon steel accounts for the key processes underlying of corrosion: chemical reactions in the bulk solution, electrochemical reactions at the steel surface, the mass transport between the bulk solution to the steel surface, and the corrosion product formation and growth (iron carbonate and iron sulfide). The model is able to predict the corrosion rate, as well as the surface water chemistry, as related to all of the key species involved. The model has been successfully calibrated against experimental data in conditions where corrosion product layers do not form and in environments where they do, and compared to other similar models.

**KEY WORDS:** carbon dioxide, carbon steel, corrosion model, corrosion rate, hydrogen sulfide, uniform corrosion

## INTRODUCTION

Corrosion predictive models are very useful tools that can be used to determine corrosion allowances, make

predictions of facilities' remaining life, and provide guidance in corrosion management. When it comes to internal corrosion of mild steel in the oil and gas industry, the mechanism of CO<sub>2</sub> corrosion is well understood through laboratory investigations.<sup>1-2</sup> Hence, models for CO<sub>2</sub> corrosion developed in the past range from those based on empirical correlations to mechanistic models describing the different processes involved in CO<sub>2</sub> corrosion of carbon steel. In 2002, Nyborg<sup>3</sup> published a performance-based review of several CO<sub>2</sub> corrosion models focusing on the ability to account for effects of pH, protective iron carbonate layers, oil wetting, fluid flow, H<sub>2</sub>S, top-of-the-line corrosion, and acetic acid. Some five years later, Nešić published a comprehensive review of the understanding and modeling practices for internal corrosion of oil and gas pipelines.<sup>4</sup>

In the case of H<sub>2</sub>S corrosion, there are numerous experimental studies; however, the mechanism of H<sub>2</sub>S corrosion is still unclear and only a few models have been developed and published in the open literature for pure H<sub>2</sub>S or mixed CO<sub>2</sub>/H<sub>2</sub>S corrosion. It has been widely observed that the uniform corrosion rate is reduced in the presence of very small concentrations of H<sub>2</sub>S (1 mbar [0.1 kPa] or even smaller) at room temperature and higher. To account for this effect, one approach is to use a factor related to H<sub>2</sub>S concentration and correct the predicted sweet (CO<sub>2</sub>) corrosion rate. For example, in 1999 Anderko, et al.,<sup>5</sup> developed a mechanistic model to predict the corrosion rates of carbon steel in both CO<sub>2</sub>- and H<sub>2</sub>S-containing environments, which included a thermodynamic calculation to predict corrosion product composition and an electrochemical corrosion model to simulate the

Submitted for publication: February 10, 2015. Revised and accepted: January 20, 2016. Preprint available online: January 21, 2016, <http://dx.doi.org/10.5006/1667>.

<sup>‡</sup> Corresponding author. E-mail: nesic@ohio.edu.

\* Institute for Corrosion and Multiphase Technology, Department of Chemical and Biomolecular Engineering, Ohio University, 342 W. State St., Athens, OH 45701.

processes of cathodic and anodic reactions on the steel surface. To get the desired performance, the predictions of the electrochemical model were simply correlated to the final steady state corrosion rate experimental data by using a surface coverage factor of iron sulfide and iron carbonate. Mechanistic verification of this approach using electrochemical kinetics data was not performed, and the water chemistry at the steel surface and in the bulk solution was not distinguished in their model. In 2009, Sun and Nešić<sup>2,6</sup> modeled CO<sub>2</sub>/H<sub>2</sub>S corrosion based on an assumption that in the presence of H<sub>2</sub>S, the corrosion rate is always mass transfer controlled as a result of the ubiquitous presence of iron sulfide layers. A wide range of experimental results were collected to calibrate this model, making it a useful tool for the prediction of transient corrosion rates arising from the growth of iron sulfide layers. However, the model consisted of a number of assumptions that were not explicitly verified. In particular, it was universally assumed that the rate of corrosion in the presence of H<sub>2</sub>S is always under mass transfer control; hence, the electrochemical reactions were not defined nor included in the model. This made it harder to integrate this model with mechanistic (electrochemical) models of CO<sub>2</sub> corrosion.

In earlier papers published by the present authors, an electrochemical corrosion model<sup>7-8</sup> of H<sub>2</sub>S corrosion without iron sulfide layer growth has been developed to describe the corrosion process on a bare steel surface, thereby avoiding the complex issues associated with formation and growth of an iron sulfide corrosion product layer. The model in the present paper is mainly focused on the growth and the effect of protective corrosion product layers (iron carbonate or iron sulfide) on the corrosion by taking a mechanistic approach. The model is able to predict the corrosion rate and also the concentration at the metal surface of all of the species involved in the corrosion process.

## PHYSICOCHEMICAL PROCESSES UNDERLYING CO<sub>2</sub>/H<sub>2</sub>S CORROSION

CO<sub>2</sub>/H<sub>2</sub>S corrosion is a complex process involving multiple physicochemical processes occurring simultaneously. These are: chemical reactions in the bulk solution, mass transport of aqueous species through the liquid boundary layer and the porous surface layer, electrochemical reactions at the steel

surface, and porous corrosion product layer formation which may or may not be protective. All of these processes must be taken into account in a predictive model to provide a realistic estimation of the corrosion rate. For CO<sub>2</sub> corrosion, an electrochemical mechanistic model<sup>9-10</sup> based on the key physicochemical processes has been developed and implemented into a software package that is well known and freely available.<sup>11</sup> For H<sub>2</sub>S corrosion, Sun and Nešić's mass transfer model<sup>6</sup> is also publically available and widely implemented.<sup>2,11</sup> Based on the recent experimental findings,<sup>12</sup> and the more thorough understanding that has emerged in the meantime, a more comprehensive uniform aqueous H<sub>2</sub>S corrosion model can now be formulated and is described next.

The outline of the new physicochemical model can be started by picturing aqueous H<sub>2</sub>S diffusing to a steel surface, where it reacts rapidly to form a very thin adsorbed sulfide layer, as suggested by Marcus, et al.<sup>13</sup> Following the mechanism proposed by Smith and Wright,<sup>14</sup> it can be written as:



The work of Marcus, et al.,<sup>13</sup> indicates that sulfur adsorbs very strongly to a steel surface and can displace adsorbed H<sub>2</sub>O and OH<sup>-</sup>. This action results in slowing down the kinetics of electrochemical reactions such as Fe dissolution, H<sub>2</sub>O reduction, and carbonic acid reduction, apparently by affecting the double layer. The electrochemical reactions (both anodic and cathodic) continue to go forward despite an existing adsorbed sulfide layer, albeit at a slower rate.

When the surface concentrations of Fe<sup>2+</sup> and S<sup>2-</sup> ions exceed the solubility limit of iron sulfide (initially mackinawite), solid iron sulfide is thermodynamically stable, and it will precipitate on the steel surface:



This iron sulfide layer can grow and retard the corrosion rate via a surface coverage effect and a mass transfer effect (acting as diffusion barrier). The present transient corrosion model is somewhat similar, but also quite different from the model proposed by Sun and Nešić<sup>6</sup> in some key elements. A comparison between the key differences for the two models is listed in Table 1.

**TABLE 1**  
*Differences Between Sun-Nešić Model<sup>6</sup> and the Present Model*

Sun-Nešić Model (2009) <sup>6</sup>	Present Model
A thin inner mackinawite film formed by direct chemical reaction acting as a solid state diffusion barrier.	A thin adsorbed iron sulfide film affecting directly the kinetics of different electrochemical reactions (retardation effect).
A porous outer iron sulfide layer formed by spalling of the inner layer. Corrosion rate is always under mass-transfer control because of the porous outer iron sulfide layer and inner mackinawite film.	An outer iron sulfide layer formed via a precipitation mechanism. Corrosion rate is not always under mass-transfer control depending on the kinetics of mass transfer and electrochemical reactions.

## MODEL DESCRIPTION

The present model describes H<sub>2</sub>S/CO<sub>2</sub> corrosion in terms of two main processes: an electrochemical corrosion process including effect of mass transport from bulk to the surface, and corrosion product formation and growth process for iron carbonate and iron sulfide.

### Electrochemical Corrosion Model

The concentration of the species can be very different in the bulk solution and at the corroding steel surface because of corrosion, mass transfer effects, and chemical reactions. One usually knows (or can readily calculate) the bulk species concentration; however, the electrochemical corrosion process depends on the surface concentrations. Therefore, the surface concentrations need to be estimated by calculation. In the present model, two calculation “nodes” were used in the computational domain: one for the species concentrations in the bulk solution and the other for the species concentrations in the thin water layer adjacent to the corroding steel surface. The concentrations of chemical species in the bulk solution can be calculated using a standard water chemistry equilibrium model. The concentrations of species at the corroding steel surface need to be calculated in a way that ensures that all of the key physicochemical processes that affect the surface concentrations are accounted for (see Figure 1). These are:

- (1) Homogenous chemical reactions close to the steel surface.
- (2) Electrochemical reactions at the steel surface.
- (3) Transport of species between the steel surface and the bulk, including convection and diffusion through the boundary layer, as well as electromigration resulting from establishment of electrical potential gradients.

These three physicochemical processes are interconnected and can be expressed by writing a material balance or mass conservation reaction for a thin surface water layer.

$$\frac{\partial c_{\text{surface},j}}{\partial t} = \frac{N_{e,j} - N_{w,j}}{\Delta x} + R_j \quad (3)$$

where  $c_{\text{surface},j}$  is the concentration of species  $j$ ,  $N_{e,j}$  is the flux of species  $j$  on the east boundary resulting from mass transfer from the bulk solution to the surface,  $N_{w,j}$  is the flux of species  $j$  on the west boundary resulting from electrochemical reactions at the steel surface, and  $R_j$  is the source/sink term resulting from homogeneous chemical reactions involving species  $j$ .

*Homogenous Chemical Reactions* — The homogenous reactions considered in the present model are well known and readily available in the open literature.<sup>1-2,9</sup> The reactions describe the interaction between various species (H<sub>2</sub>S, HS<sup>-</sup>, S<sup>2-</sup>, CO<sub>2</sub>, H<sub>2</sub>CO<sub>3</sub>, HCO<sub>3</sub><sup>-</sup>, CO<sub>3</sub><sup>2-</sup>, OH<sup>-</sup>, and H<sup>+</sup>).

It should be noted that chemical reactions are often very rapid when compared to other processes involved in corrosion, such as species transport and electrochemical reactions, thus preserving chemical equilibria throughout the solution. On the other hand, in the case of slow chemical reactions (such as the CO<sub>2</sub> hydration reaction), other faster processes can lead to local non-equilibrium conditions at the corroding steel surface. Therefore, chemical reactions can significantly affect the rates of electrochemical processes at the steel surface and then ultimately, the corrosion rate.

In order to better understand how the rates of homogenous chemical reactions are calculated in the present model, one is referred to papers by Nešić, et al.<sup>1-2,9</sup>

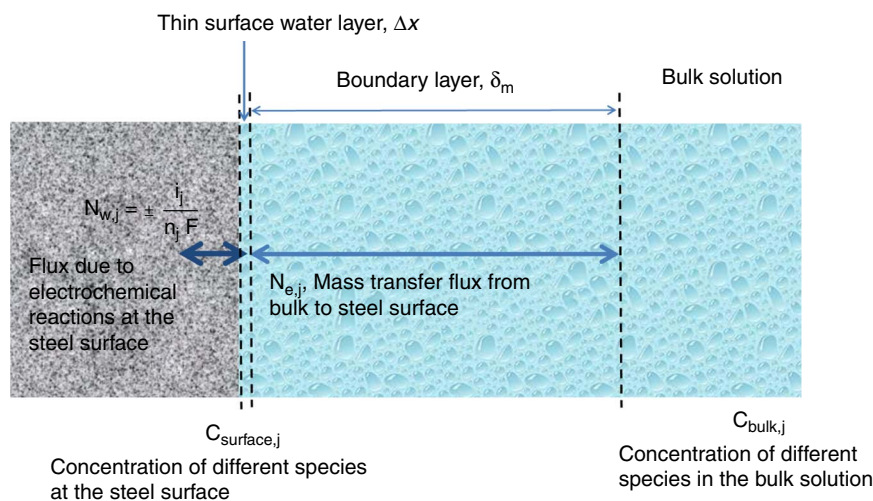
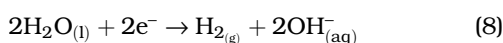
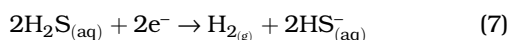
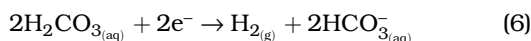
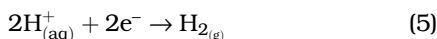
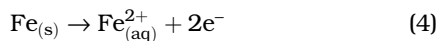


FIGURE 1. Illustration of computation domain and governing reactions for mass transport simulation.

*Electrochemical Reactions at the Steel Surface* — Electrochemical reactions at the steel surface considered in the present model include:



The Tafel equation used to calculate the current densities (rate) of various electrochemical reactions listed above is described in detail in previously published papers on the electrochemical corrosion model.<sup>7,15</sup>

$$i = i_0 10^{\pm \frac{E-E_0}{b}} \quad (9)$$

where  $i$  represents the reaction current density in  $\text{A}/\text{m}^2$ ,  $i_0$  represents a reference current density in  $\text{A}/\text{m}^2$ ,  $E$  represents the corrosion potential of the steel in V,  $E_0$  represents a reference potential in V, and  $b$  represents the Tafel slope in V/decade. In this model, the current density for each electrochemical reaction depends on the surface concentration of species, which is not explicitly known and needs to be calculated, as explained below. For a spontaneous corrosion process, the unknown corrosion potential of the steel,  $E$ , can be calculated from the charge balance reaction at the steel surface:

$$\sum_{\text{cathodic}} i = \sum_{\text{anodic}} i \quad (10)$$

Details of this calculation have already been explained elsewhere.<sup>7,15</sup> Then, the flux at the steel surface can be determined from:

$$N_{w,j} = \pm \frac{i_j}{n_j F} \quad (11)$$

where  $n_j$  is the number of mol of electrons exchanged per mol of species  $j$  participating in a particular electrochemical reaction. For species  $j$  consumed by electrochemical reactions at the steel surface, the positive sign is applied. For species  $j$  produced by electrochemical reactions at the steel surface, the negative sign is applied. For those species  $j$  that are not involved in the electrochemical reactions,  $i_j = 0$ . Once the corrosion potential ( $E$ ) is found, the partial current ( $i_j$ ) for a given species  $j$  is readily calculated from Reaction (9).

*Species Surface Concentration and Mass Transfer* — Ten minor species ( $\text{H}_2\text{S}$ ,  $\text{HS}^-$ ,  $\text{S}^{2-}$ ,  $\text{CO}_2$ ,  $\text{H}_2\text{CO}_3$ ,  $\text{HCO}_3^-$ ,  $\text{CO}_3^{2-}$ ,  $\text{OH}^-$ ,  $\text{H}^+$ , and  $\text{Fe}^{2+}$ ) and two major species ( $\text{Na}^+$  and  $\text{Cl}^-$ ) were accounted for by calculating their

mass transfer flux between the bulk solution and the steel surface. The terms “major” and “minor” refer to the magnitude of species concentration, with  $\text{Na}^+$  and  $\text{Cl}^-$  exceeding the concentration of other species by orders of magnitude. It should be noted that the concentrations of species are not calculated throughout the mass transfer boundary layer, as is done in more advanced models presented by Nešić, et al.,<sup>9-10</sup> because of inherent complexities associated with this approach. Rather, only two calculation nodes are used, one in the bulk and the other at the steel surface, so the mass transfer flux between the bulk solution to the steel surface can be calculated for each of the species using a mass transfer coefficient,  $k_{m,j}$ , approach:

$$N_{e,j} = k_{m,j}(c_{\text{bulk},j} - c_{\text{surface},j}) + k_{m,j} \frac{z_j F}{RT} c_{\text{bulk},j} \Delta\Phi \quad (12)$$

Here  $c_{\text{bulk},j}$  is the concentration of the species  $j$  in the bulk solution,  $c_{\text{surface},j}$  is the concentration of the species  $j$  at the steel surface, and  $z_j$  is the electric charge of species  $j$ . The mass transfer coefficient of species  $j$ ,  $k_{m,j}$ , can be calculated from well-known correlations such as the one for a rotating cylinder electrode proposed by Eisenberg:<sup>16</sup>

$$\text{Sh} = \frac{k_{m,j} d}{D_j} = 0.0791 \text{Re}^{0.7} \text{Sc}^{0.356} \quad (13)$$

or for turbulent single phase pipe flow, the mass transfer coefficient can be calculated by a straight pipe correlation of Berger and Hau:<sup>17</sup>

$$\text{Sh} = \frac{k_{m,j} d}{D_j} = 0.0165 \text{Re}^{0.86} \text{Sc}^{0.33} \quad (14)$$

where  $\text{Sh}$  is the Sherwood number,  $d$  is the cylinder electrode diameter or pipe diameter (m),  $D_j$  is the diffusion coefficient of various species ( $\text{m}^2/\text{s}$ ),  $\text{Re}$  is the Reynolds number =  $\rho u d / \mu$ , and  $\text{Sc}$  is the Schmidt number =  $\mu / \rho D_j$ .

The last term in the transport Reaction (11) represents electromigration resulting from a small electrical potential ( $\Delta\Phi$ ) difference between the bulk solution and the surface water layer, which is significant only for the transport of major species ( $\text{Na}^+$  and  $\text{Cl}^-$ ).

Substitution of flux density resulting from electrochemical reactions and mass transfer processes into mass conservation reaction of Reaction (3) yields the final transport reaction which can be written for each species:

$$\Delta x \frac{\partial C_{\text{surface},j}}{\partial t} = \pm \frac{i_j}{n_j F} + k_{m,j}(c_{\text{bulk},j} - c_{\text{surface},j}) + k_{m,j} \frac{z_j F}{RT} c_{\text{bulk},j} \Delta\Phi + \Delta x \cdot R_j \quad (15)$$

There are 13 unknowns (12 unknown surface concentrations and the potential gradient,  $\Delta\Phi$ ), and only 12 transport reactions. Because the aqueous solution is always charge neutral, the electroneutrality reaction must be satisfied:

$$\sum z_j C_{\text{surface},j} = 0 \quad (16)$$

The concentration for all of the considered chemical species at the steel surface can now be calculated by solving these 13 reactions. At the same time, the corrosion current and the corrosion potential are calculated using Reactions (9) and (10).

### Model of Corrosion Product Layer Growth

From the electrochemical corrosion model described in the previous section, the surface water chemistry (the concentration of different chemical species at the steel surface) and the corrosion potential of the steel are obtained. Using this information, a thermodynamic model can be used to predict which solid corrosion product may form on the steel surface (solubility calculation).<sup>18-19</sup> If this calculation suggests that solubility of a given salt is not exceeded, the corrosion process at the bare steel surface proceeds unimpeded. If any given solubility is exceeded, a corrosion product layer forms on the steel surface. The formation of the corrosion product layer may significantly affect the corrosion process. Therefore, a corrosion product layer growth model, which focuses on kinetics of iron sulfide and iron carbonate formation, was developed to address this issue. In the current model, the spalling of the corrosion product layer resulting from possible internal stress or flow was not considered, which can be addressed in future work.

In the corrosion model described above, two nodes were considered in the computational domain for species concentration calculation: one in the bulk solution and the other at the steel surface. When a corrosion product layer forms, one more node needs to be added to account for this, as shown in Figure 2.

Formation of an iron sulfide and/or iron carbonate corrosion product layer affects the fluxes and thereby the concentrations of species at the steel surface, which in turn changes the kinetics of the electrochemical processes and corrosion. To reflect this, the mass conservation reaction, Reaction (3), needs to be slightly modified to read:

$$\frac{\partial \epsilon C_{\text{surface},j}}{\partial t} = \frac{N_{e,j} - N_{w,j}}{\Delta x} + R_j \quad (17)$$

Here,  $\epsilon$  is the porosity of the corrosion product layer. The rate of reaction  $R_j$  (source or sink of species  $j$ ) now includes both homogeneous chemical reactions and heterogeneous chemical reactions such as iron sulfide and/or iron carbonate precipitation. The flux of species between the bulk and the steel surface  $N_{e,j}$  is also different as it is affected by the diffusion through the porous corrosion product layer. The flux of species as a result of electrochemical reactions at the steel surface  $N_{w,j}$  is also changed because of the partial coverage of the surface by the corrosion product layer. How these three terms,  $R_j$ ,  $N_{e,j}$ , and  $N_{w,j}$  are calculated exactly, when a corrosion product layer forms, is addressed next.

**Heterogeneous Chemical Reactions** — Homogeneous reactions have been discussed in the previous section. The focus here is on two new heterogeneous chemical reactions: iron carbonate and iron sulfide formation.

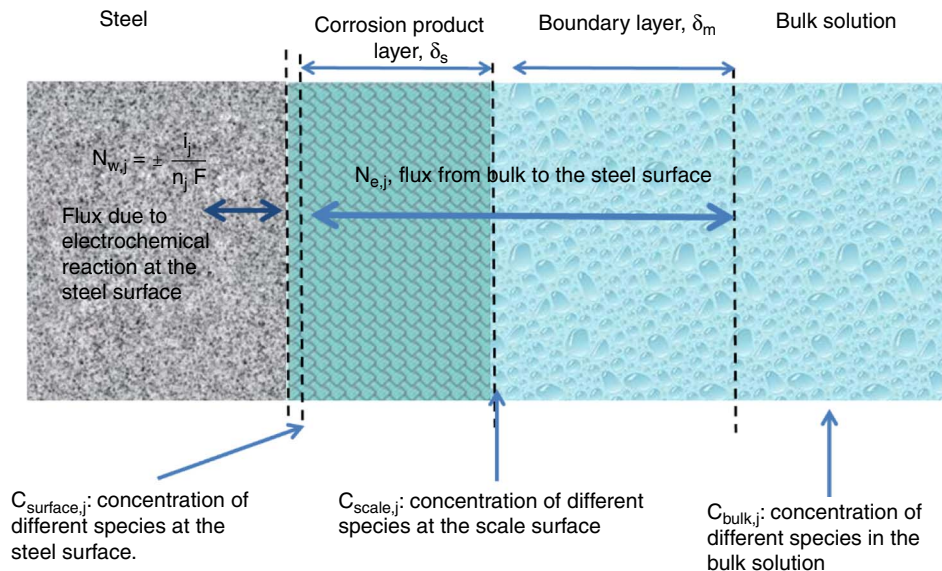


FIGURE 2. Sketch of corrosion process with corrosion product layer.

• **Iron Carbonate Formation:** Iron carbonate forms when the product of the concentrations of  $\text{Fe}^{2+}$  and  $\text{CO}_3^{2-}$  ions exceeds the solubility limit according to:



This reaction acts as a sink for  $\text{Fe}^{2+}$  and  $\text{CO}_3^{2-}$  species, and the kinetics can be calculated using Reaction (19), proposed by Sun, et al.:<sup>20</sup>

$$R_{\text{FeCO}_3(\text{s})} = e^{28.20 - \frac{64.85}{RT}} \frac{S}{V} K_{\text{spFeCO}_3} (S_{\text{FeCO}_3} - 1) \quad (19)$$

where  $R_{\text{FeCO}_3(\text{s})}$  is the precipitation rate in  $\text{mol}/(\text{m}^3 \cdot \text{s})$ ;  $\frac{S}{V}$  is the surface to volume ratio of the iron carbonate in  $1/\text{m}$ ;  $S_{\text{FeCO}_3}$  is the saturation value of iron carbonate (considering only super saturation, i.e., when  $S_{\text{FeCO}_3} > 1$ ), and  $K_{\text{spFeCO}_3}$  is the solubility limit of iron carbonate in  $(\text{mol}/\text{L})^2$ , which is given by Reaction (20).<sup>21</sup>

$$\log K_{\text{spFeCO}_3} = -59.3498 - 0.041377T - \frac{2.1963}{T} + 24.5724 \log T + 2.518I^{0.5} - 0.657I \quad (20)$$

where  $T$  is the temperature in K and  $I$  is the ionic strength in  $\text{mol}/\text{L}$ .

• **Iron Sulfide Formation:** The iron sulfide layer forms when the product of the concentrations of  $\text{Fe}^{2+}$  and  $\text{S}^{2-}$  ions exceeds the solubility limit according to Reaction (2),  $\text{Fe}_{(\text{aq})}^{2+} + \text{S}_{(\text{aq})}^{2-} \rightleftharpoons \text{FeS}_{(\text{s})}$ .

The precipitation kinetics are much faster for iron sulfide than for iron carbonate and the solubility limit is lower. Therefore, in the present model, when an iron sulfide layer can precipitate ( $S_{\text{FeS}} > 1$ ), iron carbonate precipitation is not considered. Although some previous researchers<sup>22-23</sup> have addressed the precipitation kinetics of iron sulfide, a reliable expression for the precipitation kinetics is still elusive. A new expression is suggested here, which is similar in essence to the one for iron carbonate precipitation kinetics:

$$R_{\text{FeS}(\text{s})} = e^{48 - \frac{40,000}{RT}} \frac{S}{V} K_{\text{sp,S}^{2-}} (S_{\text{FeS}} - 1) \quad (21)$$

In this expression, the constants were calibrated with the experimental results from the present study (shown later) and by using Harmandas, et al.<sup>22</sup> The saturation value for iron sulfide is denoted by  $S_{\text{FeS}}$ , and  $K_{\text{sp,S}^{2-}}$  is the solubility limit of iron sulfide in  $(\text{mol}/\text{L})^2$ , which can be calculated from Benning, et al.:<sup>24</sup>

$$K_{\text{sp,S}^{2-}} = 10^{\frac{2.848,779}{T} - 6.347} K_{\text{hs}} K_{\text{bs}} \quad (22)$$

Here,  $K_{\text{hs}}$  and  $K_{\text{bs}}$  are the equilibrium constants for the  $\text{H}_2\text{S}$  first dissociation and second dissociation, which are obtained from the open literature.<sup>25-26</sup>

*Effect of Corrosion Product Layer on Electrochemical Reactions* — The electrochemical reactions are mainly affected by the surface coverage effect where the corrosion product layer makes parts of the steel surface unavailable for corrosion. Assuming the surface coverage is equal to the volumetric porosity of the corrosion product layer,<sup>(1)</sup> the current density of each electrochemical reaction (Reaction [9]) now becomes:

$$i = i_0 10^{\frac{E-E_0}{b}} \quad (23)$$

Based on the change in the current density, the flux  $N_{e,j}$  at the steel surface can be calculated using Reaction (11). The rate of the electrochemical reactions is also affected by the changes in surface concentrations of various species resulting from retarded mass transfer through the porous corrosion product layer, as described next.

*Effect of Porous Corrosion Product Layer on Mass Transfer* — The governing reactions used to quantify the mass transfer process through the corrosion product layer for different species are similar to those described by Nešić, et al., in 2003.<sup>9</sup> The retardation of mass transfer depends primarily on the properties of the corrosion product layer, such as the thickness, porosity, and tortuosity. Considering the models available in the open literature, the mass transfer coefficient  $k_{s,j}$  of species  $j$  through the porous corrosion product layer is a function of the diffusion coefficient ( $D_j$ ), porosity ( $\epsilon$ ), tortuosity ( $\tau$ ), and thickness ( $\delta_s$ ) of the corrosion product layer.<sup>27-30</sup>

$$k_{s,j} = \frac{\epsilon \tau D_j}{\delta_s} \quad (24)$$

The tortuosity ( $\tau$ ) is taken to be proportional to the square root of porosity, in an analogy with the theory of porous electrodes.<sup>31</sup> The total mass transfer coefficient from the bulk solution to the steel surface is represented by  $k_{T,j}$ , which is the function of  $k_{m,j}$  and  $k_{s,j}$ :

$$\frac{1}{k_{T,j}} = \frac{1}{k_{s,j}} + \frac{1}{k_{m,j}} \quad (25)$$

The corrosion product layer thickness  $\Delta\delta_s$  change over time is calculated as follows:

• When iron sulfide layer forms:

$$\Delta\delta_s = \frac{\Delta x R_{\text{FeS}(\text{s})} M_{\text{FeS}} \Delta t}{\rho_{\text{FeS}} (1 - \epsilon)} \quad (26)$$

• When iron carbonate layer forms:

$$\Delta\delta_s = \frac{\Delta x R_{\text{FeCO}_3(\text{s})} M_{\text{FeCO}_3} \Delta t}{\rho_{\text{FeCO}_3} (1 - \epsilon)} \quad (27)$$

<sup>(1)</sup> Porosity is a volumetric measure of how much open space there is in the corrosion product layer. The surface coverage is a measure of how much open steel surface is available for electrochemical reactions (i.e., the surface not covered by the corrosion product layer), which can be thought of as a "superficial measure of porosity." In the absence of better data, the two measures of porosity (one volumetric, the other superficial) can be assumed to be the same.

Here  $M_{\text{FeS}}$  and  $M_{\text{FeCO}_3}$  represent the molecular weight of iron sulfide and iron carbonate (kg/mol),  $\Delta t$  is the time step, and  $\rho_{\text{FeS}}$  and  $\rho_{\text{FeCO}_3}$  are the density of iron sulfide and iron carbonate (kg/m<sup>3</sup>).

The change in surface corrosion layer porosity  $\varepsilon$  is calculated explicitly using a corrosion product layer growth model developed by Nešić, et al.,<sup>10</sup> as shown by mass balance reactions (28) and (29). The detailed derivation of these reactions is explained in the original paper and will not be repeated here.

- For the iron carbonate layer:

$$\frac{\partial \varepsilon}{\partial t} = - \frac{M_{\text{FeCO}_3}}{\rho_{\text{FeCO}_3}} R_{\text{FeCO}_3} - CR \frac{\partial \varepsilon}{\partial x} \quad (28)$$

- For the iron sulfide layer:

$$\frac{\partial \varepsilon}{\partial t} = - \frac{M_{\text{FeS}}}{\rho_{\text{FeS}}} R_{\text{FeS}} - CR \frac{\partial \varepsilon}{\partial x} \quad (29)$$

At the interface between corrosion product layer and steel surface,  $\varepsilon$  is taken to be 1, as the corrosion process continuously creates voids underneath the corrosion product layer. The initial porosity was also set as 1.

The procedure for the calculation of the corrosion rate over time is sought at discrete time steps. First, the initial corrosion rate, including surface water chemistry, is determined by the electrochemical corrosion model without the effect of any corrosion product layer. Then, a corrosion product prediction model based on thermodynamic framework is used to determine whether a corrosion product layer forms or not on the steel surface. If a corrosion product layer does not form, the calculation is over and a bare steel corrosion rate is the result. If a corrosion product layer does form, a corrosion product layer growth model is invoked. The change in porosity for the corrosion product layer is calculated from Reactions (28) or (29), and the change in thickness of layer growth is obtained from Reactions (26) or (27), depending on which corrosion products forms. Finally, the mass conservation reactions

for each species are solved. Therefore, the concentration for all of the chemical species at the steel surface can be obtained. The corrosion current, corrosion potential, corrosion rate, potential gradient in solution, and the rates (currents) for each of the cathodic reactions and the anodic reaction are calculated.

## MODEL VERIFICATION

Although the present model was primarily developed to address H<sub>2</sub>S corrosion and combined H<sub>2</sub>S/CO<sub>2</sub> corrosion, it also has the capability of predicting pure CO<sub>2</sub> corrosion. As the entire mathematical model was revised and simplified, this new model needs to be compared with other models and verified with experimental data.

### Verification of Corrosion Model Without Corrosion Product Layer

*Comparison with Other Models* — The comparison was done with two other advanced multi-node models, i.e., model presented by Nešić, et al.<sup>9-10</sup> (denoted as Model Nešić) and a corrosion model developed by Pots (denoted as Model Pots).<sup>32</sup>

For a pure CO<sub>2</sub> environment, the predicted corrosion rate, surface pH, and CO<sub>3</sub><sup>2-</sup> concentration at 25°C from these different models are shown in Figure 3. Reasonably good agreement is obtained. All three models predicted the increase of corrosion rate and the decrease of surface pH with increasing flow rate. The deviation between these three models is within 20%. Many other comparisons were made for various conditions and it was concluded that the present model is directly comparable in performance with the other two models, while being much simpler than either of them.

*Comparison with Experimental Results* — A model cannot be used with confidence before its performance is compared with experimental results. Various comparisons with laboratory data are presented next. Figure 4 shows the comparison between the present model and experimental data for an aqueous acidic

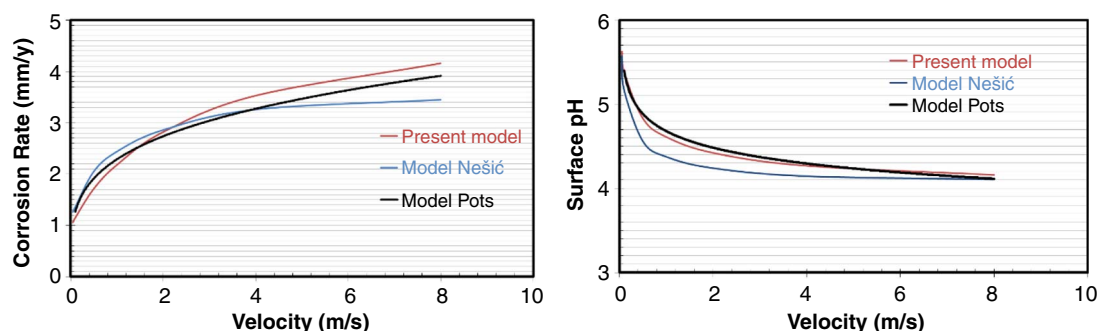


**FIGURE 3.** Comparison between the present model and two other models (Model Nešić and Model Pots) for a pure CO<sub>2</sub> environment using velocities up to 8 m/s at 25°C, [Fe<sup>2+</sup>] = 1 ppm, pH 4.0, 1 bar (100 kPa) CO<sub>2</sub>, pipeline diameter = 0.1 m, and 1 wt% NaCl.

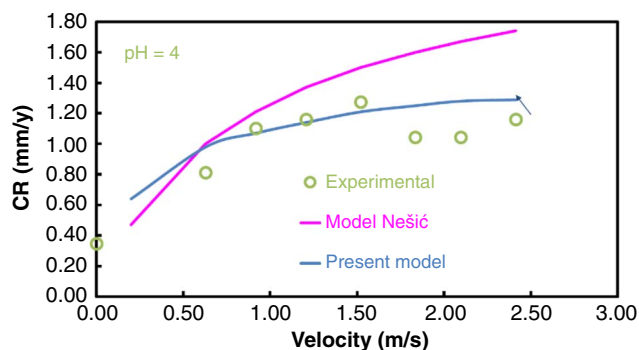


**FIGURE 4.** Comparisons between model predictions and experiment results for  $N_2$  environment,  $20^\circ C$ ,  $[Fe^{2+}] < 1$  ppm, pH 4.0, pipeline diameter = 0.01 m, and various velocities.

environment purged by  $N_2$  (without any  $CO_2$  or  $H_2S$ ) at pH 4.0 and various flow velocities. The predictions made by Model Nešić are also added to the plot, in order to get a better sense how this well-established model compared with the same experimental data. One can conclude that for a pure acidic environment, the predictions made by the present model agree reasonably well with experimental results within approximately a 20% deviation, which is better than the predictions made by Model Nešić.

For an aqueous  $CO_2$  environment, the comparison between the model predictions and experimental results for the corrosion rate obtained in glass cell and

flow systems are made by varying two important parameters: pH and velocity, as shown in Figure 5. Many other comparisons were made for a  $CO_2$  aqueous environment with similar results: a reasonable agreement was obtained within a 50% deviation. The performance of the present model was as good as that of Model Nešić. For an aqueous  $H_2S$  environment, Figure 6 shows how the present model captures the effect of  $H_2S$  concentration, flow rate, and pH. Excellent agreement is obtained. Mostly the predictions are within a 10% deviation of the experimental results, except for the very acidic pH 2 condition.

#### Verification of Corrosion Model for Conditions when Iron Carbonate Corrosion Layer Forms

Figure 7 shows the comparison of the model predictions with results of experiments conducted in a  $CO_2$  aqueous solution under flowing conditions, for conditions when protective iron carbonate corrosion product layer forms. The corrosion rate was rapidly reduced; however, these experiments are notoriously difficult to reproduce, as indicated by differences in results from five repetitions of a nominally identical experiment. The model predictions are within the range of the variation of experimental data, and are similar to those made by Model Nešić. This indicates that the present model is capable of simulating the iron carbonate layer growth kinetics and the effect on the  $CO_2$  corrosion rate.

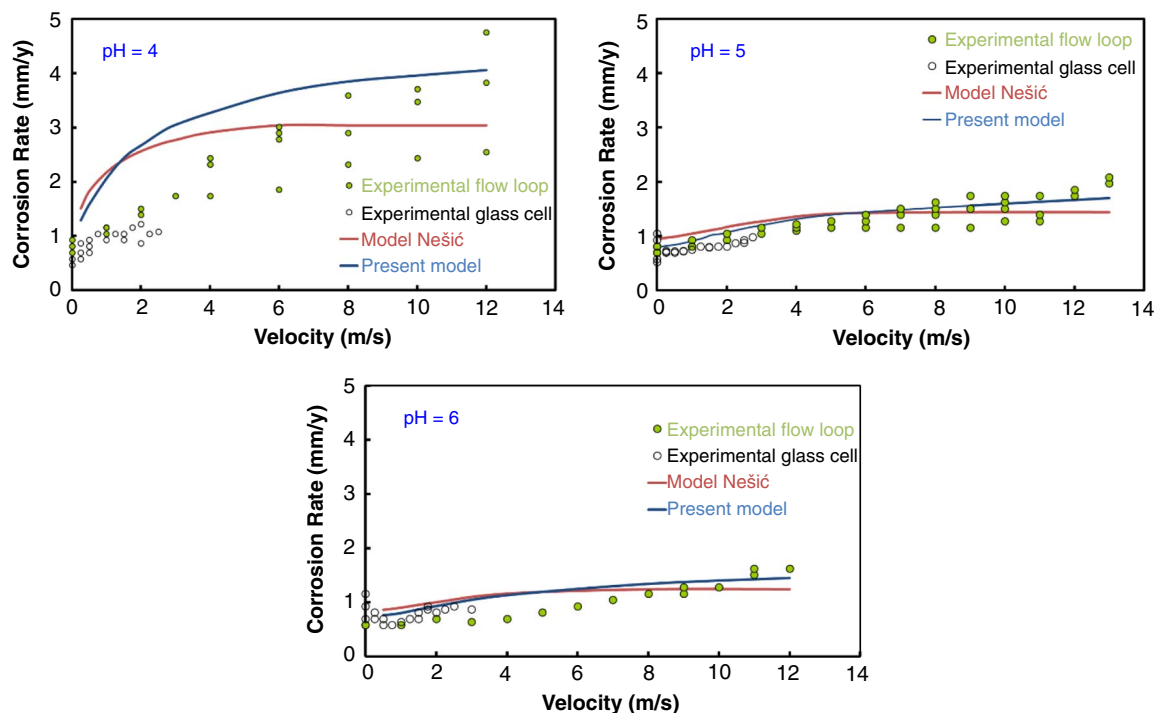


**FIGURE 5.** Comparisons between model predictions and experiment results at 1 bar (100 kPa)  $CO_2$ ,  $20^\circ C$ , various pH, and various velocities.

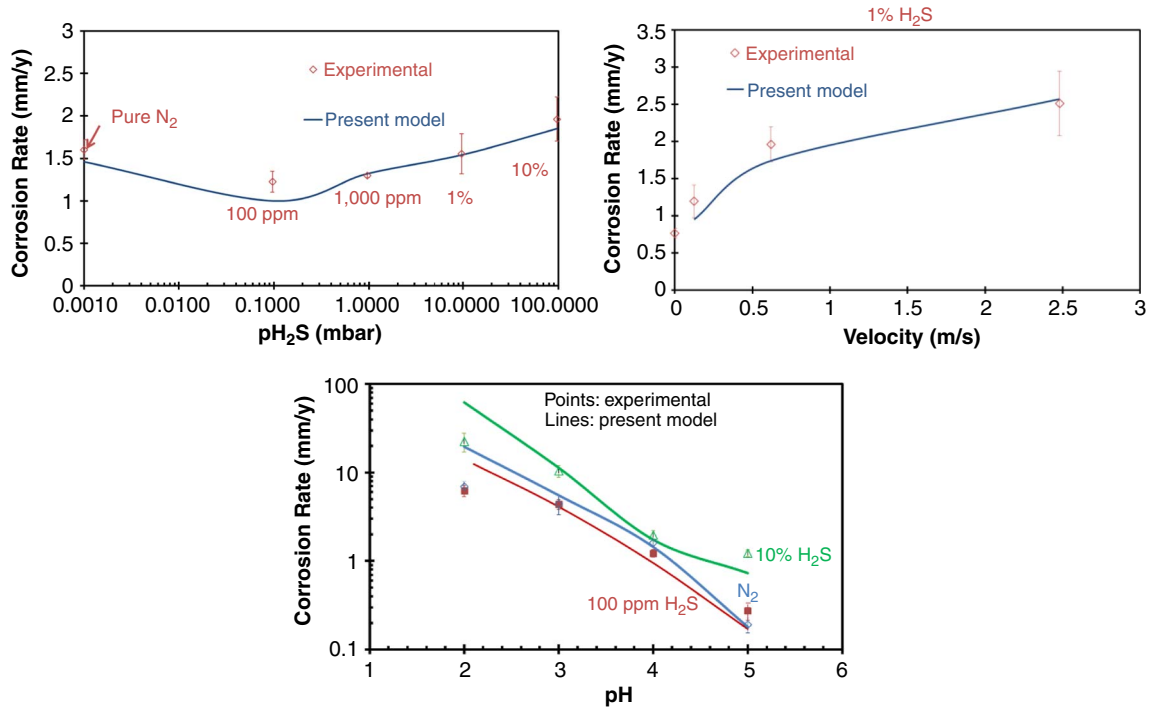


**FIGURE 6.** Comparisons between model predictions and experiment results for 30°C, 1 bar (100 kPa) total pressure, and various  $H_2S$  concentrations, velocities, and pH.

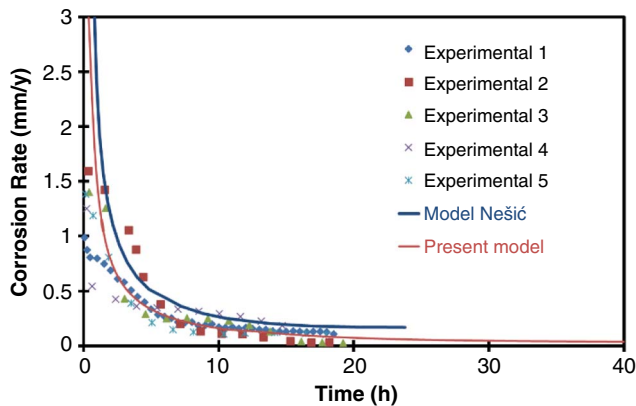


**FIGURE 7.** Comparisons between the model predictions and the experiment results for iron carbonate layer forming condition at pH 6.6, 80°C, 0.53 bar (53 kPa)  $CO_2$ , and 1,000 rpm rotating speed, 50 ppm bulk  $Fe^{2+}$ . Data is taken from the ICMT (Institute for Corrosion and Multiphase Technology) database.

### Verification of Corrosion Model for Conditions when Iron Sulfide Layer Forms

**Effect of  $pH_2S$**  — The partial pressure of  $H_2S$  is directly related to the aqueous  $H_2S$  concentration in the solution, and is an important factor as it plays dual roles. First, aqueous  $H_2S$  is a corrosive species accelerating the corrosion rate by enhancing the cathodic reaction rate. Second,  $H_2S$  also promotes the rate of the iron sulfide precipitation that decreases the general corrosion rate.

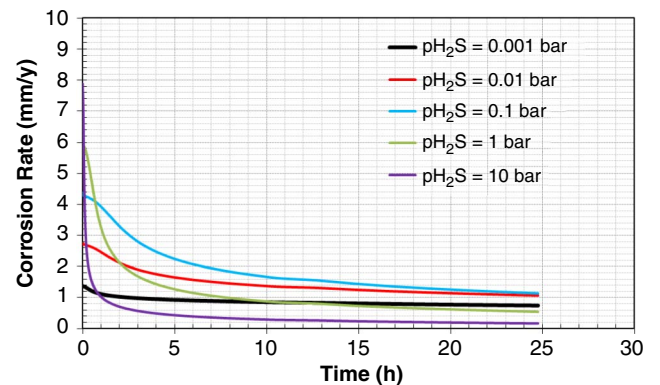


**FIGURE 8.** The predicted effect of  $pH_2S$  on the corrosion rate from present model for pH 5.0,  $T = 80^\circ C$ , and  $V = 1$  m/s.

Figure 8 illustrates the predicted effect of  $pH_2S$  on the corrosion rate calculated by the present model. The initial corrosion rate increases with increasing  $pH_2S$ ; because no corrosion product layer protectiveness is accounted for at the initial time (time zero), the system is overwhelmed by the accelerating role of  $H_2S$  reduction. However, during longer reaction times, such as 1 d, the formation of a protective iron sulfide layer is promoted by  $pH_2S$ . The best example of the dual roles of  $H_2S$  is that at 10 bar (1,000 kPa)  $pH_2S$ , the initial corrosion rate is the highest, but the corrosion rate after 1 d is the lowest.

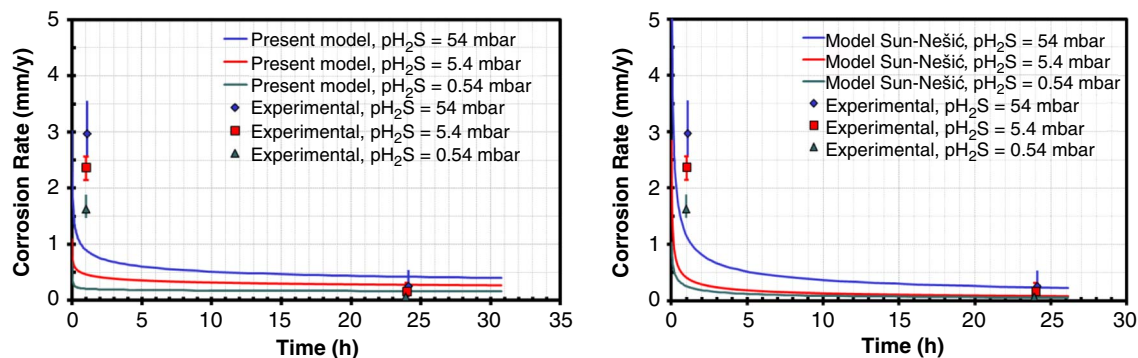


**FIGURE 9.** Corrosion rate changing with time at different  $H_2S$  partial pressure from present model and Model Sun-Nešić. Points: experimental data, lines: model predictions. Conditions: total pressure = 1 bar (100 kPa),  $H_2S$  gas partial pressure from 0.54 mbar to 54 mbar (0.054 kPa to 5.4 kPa), 80°C, experiment duration 1 h to 24 h, pH 5.0 to 5.5, stagnant. Experimental data taken from Sun.<sup>6</sup>

The model by Sun-Nešić<sup>6</sup> of  $H_2S$  corrosion was a precursor to the current work, as described earlier. Both models, the Model Sun-Nešić and the present model, were compared with the experimental data, as shown below. First, the performance at low partial pressures of  $H_2S$  was examined. The test was conducted by Sun<sup>6</sup> at  $H_2S$  gas partial pressures from 0.54 mbar to 54 mbar (0.054 kPa to 5.4 kPa). Figure 9 shows that both the present model and Model Sun-Nešić capture the corrosion rate change well.

Corrosion experiments at higher  $pH_2S$  ( $pH_2S = 16.1$  bar [1,610 kPa] in the mixed  $H_2S/N_2$  environment) were reported by Liu, et al.,<sup>33</sup> and model predictions are compared with the experimental results in Figure 10. The present model performs much better than Model Sun-Nešić at this condition.

A similar range of  $H_2S$  partial pressures were reported by Bich, et al.,<sup>34</sup> with the main difference being the presence of  $CO_2$ . Figure 11 shows the comparison between the model prediction and experimental results in a mixed  $H_2S/CO_2$  environment. The present model captures the corrosion rate change

with time, but Model Sun-Nešić tends to overpredict the corrosion rate.

*Effect of pH* — The predicted effect of pH on the corrosion rate for a pure  $H_2S$  environment is demonstrated in Figure 12 and compared with experimental data. Corrosion rate increases with a decrease in pH as expected, as the corrosiveness of the solution increases and the solubility of iron increases as well. The decrease of corrosion rate with time is much faster at pH 6.0 as a result of the formation of a denser iron sulfide layer. The present model captures the corrosion rate change much better than Model Sun-Nešić, which does not agree well with the corrosion rates at pH values less than 5. It is worth noting that the experimental linear polarization resistance corrosion rates are much higher than the model prediction at pH 4.0. This is probably a result of the iron carbide remaining on the metal surface after corroding away the ferrite phase at pH 4.0, which can accelerate the corrosion rate by providing a more cathodic reaction area.<sup>35-36</sup> This effect is not included in the present model.

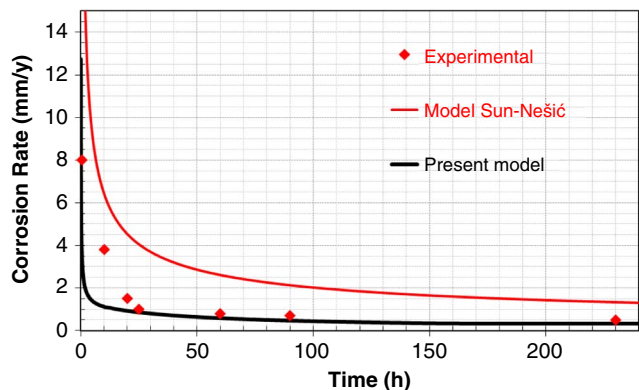


**FIGURE 10.** Corrosion rate changing with time. Points: experimental data, lines: model predictions. Conditions: 16.1 bar (1,610 kPa)  $H_2S$ , 90°C, 2 L autoclave, stagnant. Experimental data taken from Liu, et al.<sup>33</sup>

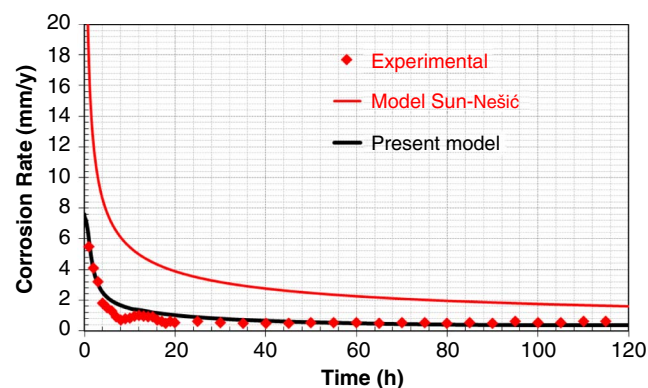


**FIGURE 11.** Corrosion rate changing with time. Points: experimental data, lines: model predictions. Conditions: 12.2 bar (1,220 kPa)  $H_2S$ , 3.5 bar (350 kPa)  $CO_2$ , 65°C. Experimental data taken from Bich, et al.<sup>34</sup>

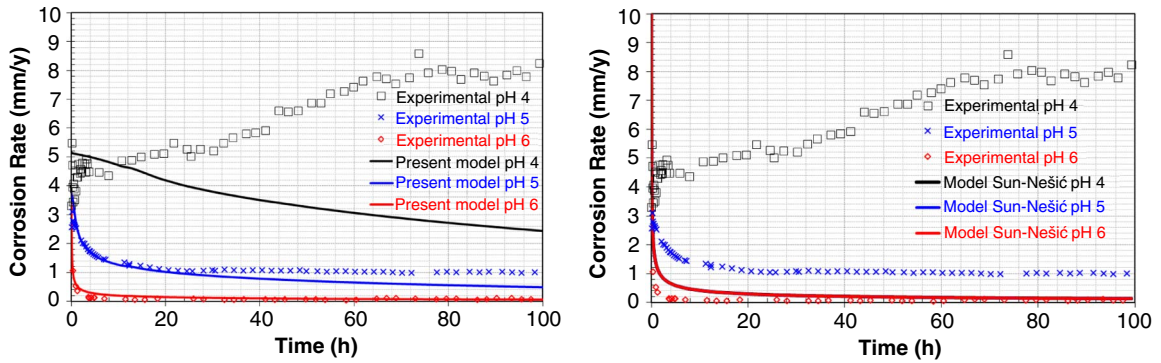
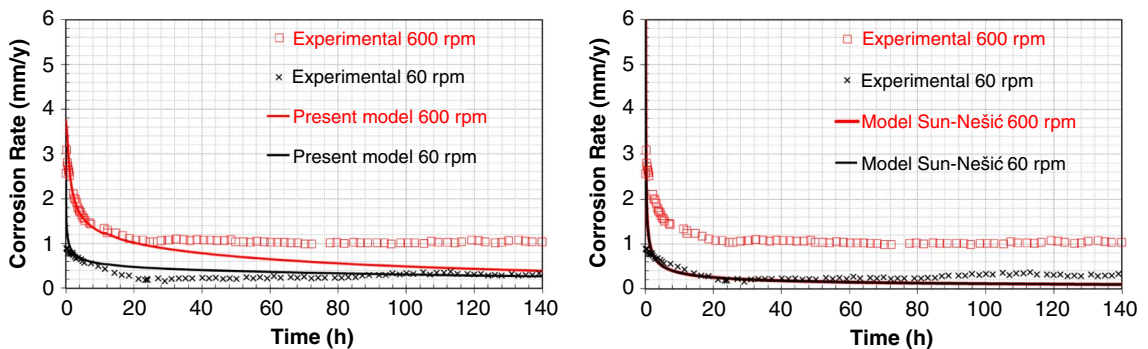


**FIGURE 12.** Corrosion rate changing with time. Points: experimental data, lines: model predictions. Conditions: 0.054 bar (5.4 kPa)  $pH_2S$ , balance nitrogen,  $T=80^{\circ}C$ , stirring rate: 600 rpm for pH 4 and pH 5, and 400 rpm for pH 6.

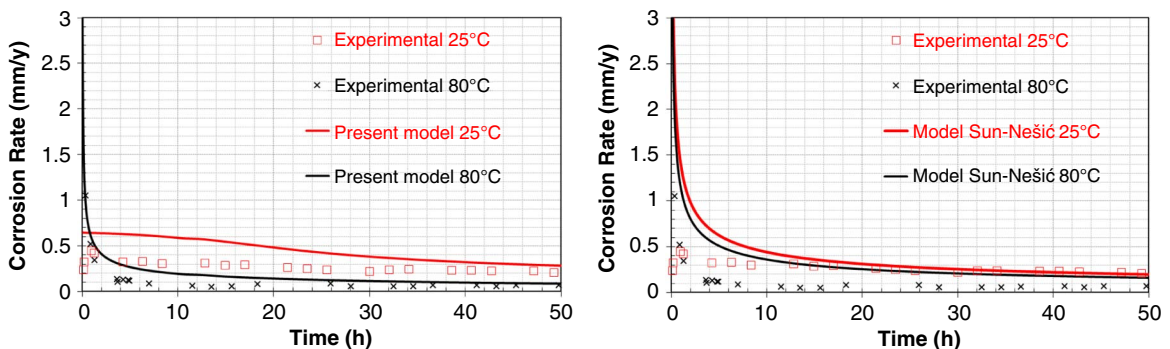
*Effect of Flow* — Fluid flow and turbulence play an important role in the corrosion process. Higher flow can increase the corrosion rate through enhancing the mass transport process, especially when there is no corrosion product layer formed. Flow can also affect the formation of a protective iron sulfide layer. Species transport in turbulent flow affects the surface concentration of species and, consequently, changes the precipitation rate of iron sulfide.

Figure 13 shows the comparisons between model predictions and experimental results at different flow conditions. The present model is generally able to predict the change of the corrosion rate rather well.

*Effect of Temperature* — Increasing temperature makes the bare steel corrosion rate higher, as seen in the beginning of the experiments shown in Figures 14 and 15. However, the formation of a protective iron



**FIGURE 13.** Corrosion rate vs. time. Points: experimental data, lines: model predictions. Conditions:  $pH_2S=0.054$  bar (5.4 kPa), balance nitrogen,  $T=80^{\circ}C$ , pH 5.0.



**FIGURE 14.** Corrosion rate vs. time. Points: experimental data, lines: model predictions. Conditions: total pressure = 1 bar (100 kPa),  $pH_2S=0.1$  bar (10 kPa) at  $25^{\circ}C$ ,  $pH_2S=0.054$  bar (5.4 kPa) at  $80^{\circ}C$ , pH 6.0, 400 rpm stirring rate. Experimental data taken from Ning.<sup>37</sup>

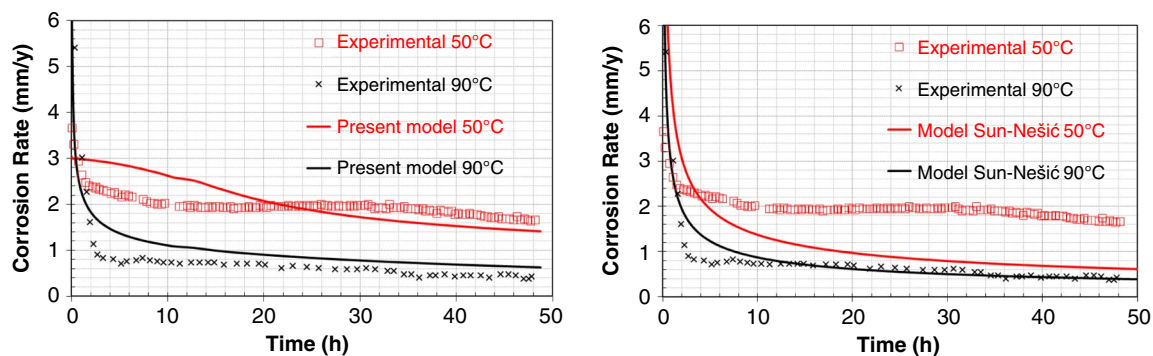


**FIGURE 15.** Corrosion rate vs. time. Points: experimental data, lines: model predictions. Conditions: total pressure = 1 bar (100 kPa),  $p_{\text{H}_2\text{S}} = 0.3$  bar (30 kPa) at 90°C,  $p_{\text{H}_2\text{S}} = 0.88$  bar (88 kPa) at 50°C, pH 4.2 to 4.7, stirring condition. Experimental data taken from Abayarathna, et al.<sup>38</sup>

sulfide layer is also promoted at high temperature, and therefore, the corrosion rate decreases more rapidly with temperature increase. Comparisons between the present model predictions and experimental results at different temperatures, shown in Figures 14 and 15, faithfully capture this behavior. Model Sun-Nešić is not sensitive to temperature because mass transfer control of the corrosion process was assumed in the model, and the mass transfer process is not as sensitive as the electrochemical and chemical reaction processes to temperature change. Therefore, Model Sun-Nešić cannot capture the higher initial corrosion and lower final corrosion at the high temperature.

## CONCLUSIONS

❖ A relatively simple mechanistic transient model of uniform  $\text{CO}_2/\text{H}_2\text{S}$  corrosion of carbon steel has been developed, which accounts for the key processes underlying corrosion:

- chemical reactions in the bulk solution,
- electrochemical reactions and chemical reactions at the steel surface,
- mass transport between the bulk solution to the steel surface, and
- corrosion product formation and growth (iron carbonate and iron sulfide).

❖ The model is able to predict the corrosion rate, as well as the surface concentration, of all key species involved in the corrosion process. The model has been successfully calibrated against experimental data in conditions where corrosion product layers do not form and in those where they do. Parametric testing of the model in iron sulfide forming conditions has been conducted in order to gain insight into the effect of various environmental parameters on the  $\text{H}_2\text{S}/\text{CO}_2$  corrosion process. Performance of the present model was favorably compared to the performance of other similar models that are publically available.

## ACKNOWLEDGMENTS

The authors would like to express sincere appreciation to the following industrial sponsors for their financial support and direction: BP, Champion Technologies, Chevron, Clariant Oil Services, ConocoPhillips, ENI S. P. A., ExxonMobil, Inpex Corporation, NALCO Energy Services, Occidental Petroleum Co., Petrobras, PETRONAS, PTT, Saudi Aramco, Total, TransCanada, MI-SWACO, HESS, and WGIM. The authors would also like to thank Dr. Bert Pots for his expert advice and providing data for the model comparison.

## REFERENCES

1. S. Nešić, "Carbon Dioxide Corrosion of Mild Steel," in *Uhlig's Corrosion Handbook*, ed. R.W. Revie, 3rd ed. (Hoboken, NJ: John Wiley & Sons, Inc., 2011), p. 229-245.
2. S. Nešić, W. Sun, "Corrosion in Acid Gas Solutions," in *Shreir's Corrosion*, ed. T.J.A. Richardson, vol. 2 (Amsterdam, Netherlands: Elsevier, 2010), p. 1270-1298.
3. R. Nyborg, "Overview of  $\text{CO}_2$  Corrosion Models for Wells and Pipelines," CORROSION 2002, paper no. 233 (Houston, TX: NACE International, 2002).
4. S. Nešić, *Corros. Sci.* 49 (2007): p. 4308-4338.
5. A. Anderko, P. McKenzie, R.D. Young, *Corrosion* 57 (2001): p. 202-213.
6. W. Sun, S. Nešić, *Corrosion* 65 (2009): p. 291-307.
7. Y. Zheng, B. Brown, S. Nešić, *Corrosion* 70 (2014): p. 351-365.
8. Y. Zheng, J. Ning, B. Brown, S. Nešić, *Corrosion* 71 (2015): p. 316-325.
9. S. Nešić, A. Stangeland, M. Nordsveen, R. Nyborg, *Corrosion* 59 (2003): p. 489-497.
10. S. Nešić, K.L.J. Lee, *Corrosion* 59 (2003): p. 616-628.
11. "FREECORP - Corrosion Prediction Software," Ohio University, 2008, <http://www.corrosioncenter.ohio.edu/software/freecorp/> (Mar. 27, 2016).
12. Y. Zheng, J. Ning, B. Brown, D. Young, S. Nešić, "Mechanistic Study of the Effect of Iron Sulfide Layers on Hydrogen Sulfide Corrosion of Carbon Steel," CORROSION 2015, paper no. 5933 (Houston, TX: NACE, 2015).
13. P. Marcus, E. Protopopoff, *J. Electrochem. Soc.* 137 (1990): p. 2709-2712.
14. S.N. Smith, E.J. Wright, "Prediction of Minimum  $\text{H}_2\text{S}$  Levels Required for Slightly Sour Corrosion," CORROSION 1994, paper no. 11 (Houston, TX: NACE, 1994).
15. Y. Zheng, J. Ning, B. Brown, S. Nešić, "Electrochemical Model of Mild Steel Corrosion in a Mixed  $\text{H}_2\text{S}/\text{CO}_2$  Aqueous Environment," CORROSION 2014, paper no. 3907 (Houston, TX: NACE, 2014).

16. M. Eisenberg, C.W. Tobias, C.R. Wilke, *J. Electrochem. Soc.* 101 (1954): p. 306-320.
17. F.P. Berger, K.-F.F.-L. Hau, *Int. J. Heat Mass Transf.* 20 (1977): p. 1185-1194.
18. J. Ning, Y. Zheng, D. Young, B. Brown, S. Nešić, *Corrosion* 70 (2014): p. 375-389.
19. T. Tanupabrungsun, "Thermodynamics and Kinetics of Carbon Dioxide Corrosion of Mild Steel at Elevated Temperatures" (Ph.D. diss., Ohio University, 2012).
20. W. Sun, "Kinetics of Iron Carbonate and Iron Sulfide Scale Formation in Carbon Dioxide/Hydrogen Sulfide Corrosion" (Ph.D. diss., Ohio University, 2006).
21. W. Sun, S. Nešić, R.C. Woollam, *Corros. Sci.* 51 (2009): p. 1273-1276.
22. N.G. Harmandas, P.G. Koutsoukos, *J. Cryst. Growth* 167 (1996): p. 719-724.
23. D. Rickard, *Geochim. Cosmochim. Acta* 59 (1995): p. 4367-4379.
24. L.G. Benning, R.T. Wilkin, H.L. Barnes, *Chem. Geol.* 167 (2000): p. 25-51.
25. O.M. Suleimenov, R.E. Krupp, *Geochim. Cosmochim. Acta* 58 (1994): p. 2433-2444.
26. Y.K. Kharaka, W.D. Gunter, P.K. Aggarwal, E.H. Perkins, J.D. Dedraal, "SOLMINEQ. 88: A Computer Program for Geochemical Modeling of Water - Rock Interactions," U.S. Geological Survey, Water-Resources Investigations Report 88-4227, 1988.
27. E.L. Cussler, *Diffusion: Mass Transfer in Fluid Systems*, 2nd ed. (Cambridge, United Kingdom: Cambridge University Press, 1997).
28. P. Grathwohl, *Diffusion in Natural Porous Media: Contaminant Transport, Sorption/Desorption and Dissolution Kinetics* (New York, NY: Springer, 1998).
29. M. Gopal, S. Rajappa, R. Zhang, "Modeling the Diffusion Effects Through the Iron Carbonate Layer in the Carbon Dioxide Corrosion of Carbon Steel," CORROSION 1998, paper no. 026 (Houston, TX: NACE, 1998).
30. D. Mu, Z.-S. Liu, C. Huang, N. Djilali, *Microfluidics Nanofluidics* 4 (2008): p. 257-260.
31. L. Pisani, *Transp. Porous Media* 88 (2011): p. 193-203.
32. B.F.M. Pots, "Mechanistic Models for the Prediction of CO<sub>2</sub> Corrosion Rates Under Multi-Phase Flow Conditions," CORROSION 1995, paper no. 137 (Houston, TX: NACE, 1995).
33. M. Liu, J. Wang, W. Ke, E.-H. Han, *J. Mater. Sci. Technol.* 30 (2014): p. 504-510.
34. N.N. Bich, K.G. Goerz, "Caroline Pipeline Failure: Findings on Corrosion Mechanisms in Wet Sour Gas Systems Containing Significant CO<sub>2</sub>," CORROSION 1996, paper no. 026 (Houston, TX: NACE, 1996).
35. J.L. Mora-Mendoza, S. Turgoose, *Corros. Sci.* 44 (2002): p. 1223-1246.
36. T. Berntsen, M. Seiersten, T. Hemmingsen, *Corrosion* 69 (2013): p. 601-613.
37. J. Ning, "Investigation of Polymorphous Iron Sulfide in H<sub>2</sub>S Corrosion of Mild Steel," Ohio University Advisory Board Meeting, Ohio University, 2013.
38. D. Abayarathna, A.R. Naraghi, S. Wang, "The Effect of Surface Films on Corrosion of Carbon Steel in a CO<sub>2</sub>-H<sub>2</sub>S-H<sub>2</sub>O System," CORROSION 2005, paper no. 417 (Houston, TX: NACE, 2005).